Laser produced plasma sources for nanolithography—Recent integrated simulation and benchmarking

A. Hassanein and T. Sizyuk

Citation: Phys. Plasmas **20**, 053105 (2013); doi: 10.1063/1.4807379
View online: http://dx.doi.org/10.1063/1.4807379
View Table of Contents: http://pop.aip.org/resource/1/PHPAEN/v20/i5
Published by the American Institute of Physics.

Laser produced plasma sources for nanolithography—Recent integrated simulation and benchmarking

A. Hassanein and T. Sizyuk
Center for Materials under Extreme Environment, School of Nuclear Engineering, Purdue University, West Lafayette 47907, USA

(Received 22 March 2013; accepted 1 May 2013; published online 21 May 2013)

Photon sources for extreme ultraviolet lithography (EUVL) are still facing challenging problems to achieve high volume manufacturing in the semiconductor industry. The requirements for high EUV power, longer optical system and components lifetime, and efficient mechanisms for target delivery have narrowed investigators towards the development and optimization of dual-pulse laser sources with high repetition rate of small liquid tin droplets and the use of multi-layer mirror optical system for collecting EUV photons. We comprehensively simulated laser-produced plasma sources in full 3D configuration using 10–50 μm tin droplet targets as single droplets as well as, for the first time, distributed fragmented microdroplets with equivalent mass. The latter is to examine the effects of droplet fragmentation resulting from the first pulse and prior to the incident second main laser pulse. We studied the dependence of target mass and size, laser parameters, and dual pulse system configuration on EUV radiation output and on atomic and ionic debris generation. Our modeling and simulation included all phases of laser target evolution: from laser/droplet interaction, energy deposition, target vaporization, ionization, plasma hydrodynamic expansion, thermal and radiation energy redistribution, and EUV photons collection as well as detail mapping of photons source size and location. We also simulated and predicted the potential damage to the optical mirror collection system from plasma thermal and energetic debris and the requirements for mitigating systems to reduce debris fluence. The debris effect on mirror collection system is analyzed using our three-dimensional ITMC-DYN Monte Carlo package. Modeling results were benchmarked against our CMUXE laboratory experimental studies for the EUV photons production and for debris and ions generation. © *2013 AIP Publishing LLC*. [http://dx.doi.org/10.1063/1.4807379]

I. INTRODUCTION

Extreme ultraviolet (EUV) photons source is probably the main obstacle in the successful development of cost effective nanolithography system for manufacturing the next generation computer chips. Currently, the EUV lithography (EUVL) community has narrowed the research and developments to two main directions: discharge produced plasma (DPP) sources assisted with trigger lasers and dual-pulse laser PP (LPP) sources using mass-limited targets. Such complex systems require extensive optimization to enhance the conversion efficiency (CE) and to significantly increase components lifetime. Detail source optimization without comprehensive understanding of all physical processes requires, however, significant experimental work and very costly efforts. Multi-dimensional computer simulations integrating all important physics in fine details with accurate numerical methods can significantly accelerate EUV source development and narrow/identify critical experiments needed to further validate and benchmark these models.

The current main design of LPP sources for efficient EUV photons production utilizes two-laser pulses (a pre-pulse followed by a main pulse after certain delay time) incident on a liquid tin droplet with certain size. The choice of the optimum droplet size, for example, is related to the performance and cost effectiveness of the entire LPP source. Reducing droplet size will reduce the fluences of energetic ions and atoms and fragments deposition on the optical mirrors system collecting these valuable EUV photons and therefore, extending mirrors lifetime. However, due to several other factors, such as the expansion of preheated and evaporated droplet from the pre-pulse to the appropriate volume and density for the optimum coupling with the main CO_2 laser[1] or due to the desired plasma volume and hydrodynamic confinement effects over a spherical target during the main laser exposure, the droplet size for efficient EUV photons production should be at least 20 μm in diameter.[2] For further optimization, from the point of view of the minimum EUV power requirements needed for high volume production manufacturing, increasing droplet size to 30 μm or larger is deemed necessary.[3] This is also important for the desired potential increase in the main laser energy for higher throughput, without loss of source efficiency, which is restricted in the case of the 20 μm droplets or smaller.[2]

We extended and enhanced our modeling and analysis of LPP sources with small droplets using Nd:YAG laser for the pre-pulse followed by CO_2 laser as the main pulse. Our previous simulations showed an increase of the CE using pre-pulse, up to 1.3% for 10-μm droplet and up to 3% for the 30-μm droplet.[3] The smaller droplets, i.e., 10 μm and 20 μm were almost entirely vaporized; this means we used the full mass of these targets for mist (vapor-plasma) creation. Vapor density was near uniformly distributed in the case of

smaller droplets before the main CO_2 laser pulse at the predicted optimum delay time between these two pulses. We predicted and used in our simulations the fourth harmonic of Nd:YAG laser for optimum droplet preheating and vaporization. We utilized the advantages of the 266 nm wavelength for the pre-pulse stage, which include much higher vaporization rate with lower pulse intensity compared to 1064 nm laser, generated less energetic ions debris, and as a result of the complete vaporization of droplet caused less contamination of the optical mirrors from tin droplet debris. In addition, as it will be shown in the detailed analysis of the produced vapor-plasma mist, the 266 nm wavelength can generate more confined plume preventing the fast escape of atoms and ions during plume evolution.

The current work in this study presents our new simulation results for LPP sources using 50-μm droplets, optimization of pre-pulse and main pulse lasers for efficient EUV output, details of droplet and fragments vaporization, and the effect of mist composition on EUV photons output and multilayer mirror (MLM) surface damage.

II. BRIEF DESCRIPTION OF THE INTEGRATED MODELS

We used our HEIGHTS simulation package to study and optimize LPP sources and to make realistic predictions as well as benchmarking of recent key experimental results. HEIGHTS package includes 3D detailed descriptions of various integrated physical processes involved in LPP devices. We used splitting methods to solve the general hydrodynamic equations set for LPP application. HEIGHTS calculates in full 3D the evolution of plasma/vapor hydrodynamics.[4] Energy dissipation due to thermal conduction and radiation transport (RT) is used as correction factor for the results of the predicted convection fluxes. The energy distribution in domain is considered separately for ions and electrons. Explicit methods and implicit with sparse linear equations solver are implemented for the solution of heat conduction equation in the condensed target and in plasma.[5] Accurate description of energy transport in plasma by radiation fluxes is very important, especially for high intensities of laser pulses. Comprehensive 3D model for RT, verified and benchmarked, is critical for correct simulation of LPP devices, particularly in predicting the collected EUV photons source. Because of the important role that RT plays in any intense power deposition on target materials, two main separate modeling approaches for detailed RT calculations were developed, verified, and compared in the frame of our HEIGHTS package for various plasma science applications.[6] These include direct integration of RT equations along photons path and Monte Carlo models with several weighting factors to enhance accuracy and reduce the extensive computational time. These approaches along with appropriate numerical techniques for multidimensional solution required for LPP applications provide significant insight on the overall EUV production, source size, and collection efficiency. Special attention is given to the calculation of plasma properties and optical coefficients, especially in narrow region, i.e., $13.5 \pm 1\%$ nm required for EUVL application. The structure of atomic energy levels, wavefunctions, transition probabilities, ionization potentials, oscillator strengths, broadening constants, photoionization cross-sections, and other atomic characteristics are calculated using the self-consistent Hartree-Fock-Slater (HFS) method implemented in HEIGHTS. The collisional-radiative equilibrium (CRE) model is used to calculate the populations of atomic levels, ionization balance, and the ion and electron plasma concentrations.[7] The absorption and emission coefficients are calculated as the sum of contributions from bound-bound, bound-free, and free-free transitions. HEIGHTS Monte Carlo models for laser energy deposition take into account laser photons interaction with solid/liquid target, with vapor and plasma including photons absorption, reflection, and reabsorption after reflection.[3,6] Detailed model for target vaporization are based on target thermophysical properties as well as the kinetics of evaporation and takes into account possibility of recondensation.[8] The developed algorithms in HEIGHTS for unstructured mesh generation allow, for example, fine resolution of most important regions in domain, e.g., around 0.1 μm cell size for the target surface. The models implemented in HEIGHTS are extensively tested and benchmarked separately in each physics phase of laser/target interaction as well as in the entire integrated system without any parameters adjustments or fitting routines.

We then finally used our ITMC-DYN (Ion Transport in Materials and Compounds) dynamic Monte Carlo package to study surface damage of the MLM optical collection system due to the energetic ions produced during the laser interaction with tin targets. The package includes Monte Carlo models for ions interaction with target atoms as well as models for particles diffusion, surface segregation, molecular recombination, and desorption for gaseous species. The integrated models are time-dependent and self-consistent among all physical processes involved with continuous dynamic updating of target layers composition to accurately simulate realistic experimental conditions.[9,10]

III. MIST CREATION FROM DROPLETS

The utilization of pre-pulses for target preparation prior to main pulse has significantly increased CE of LPP sources employing small droplets. The highest CE for CO_2 lasers without pre-pulse, obtained in experiments with droplets of up to 50 μm, is only $\sim$0.5%.[11] Similar values were predicted using our HEIGHTS simulations.[3] Variations in parameters of the CO_2 laser, i.e., increase of pulse intensity or spot size, do not significantly increase CE of such single pulse laser devices using small spherical targets. This is mainly due to the high reflection of 10.6-μm wavelength from solid/liquid tin, low critical density, and therefore lower vaporization of droplet by CO_2 laser, and less confinement of the evolved plasma plume to efficiently absorb and reabsorb (after reflection) laser photons due to the hydrodynamic motion of plasma around the droplet. The Nd:YAG laser gives higher CE from small droplets, up to 1.3%; however, it is still much lower than the CE that can be obtained from planar targets.[12]

Because of the deeper penetration of Nd:YAG laser photons in vapor/plasma plume and therefore higher energy

transmitted to the target, such laser is more suitable for the pre-pulse stage. For the same reason, the fourth harmonic of this laser can even be more efficient in preparing the plume mist before the main pulse. Below we studied in detail the evolution of vapor/plasma mist from 50-μm droplet utilizing various lasers.

Figures 1 and 2 show mass density distributions developed by pre-pulse lasers having 266 nm and 1064 nm wavelengths, respectively. In the first case, the 266 nm wavelength laser with about 10 mJ energy evaporated half of droplet. The longer 1064 nm wavelength laser evaporated approximately the same mass but with intensity of 5×10^{11} W/cm^2, utilizing 400 mJ. For such high intensity laser and based on experimental results, we implemented droplet fragmentation during the laser pulse in our simulation. Therefore, we modeled droplet splitting during the 10 ns laser into many fragments and their distribution with expanding velocity of ~1 km/s predicted by recent experiments.[13]

With the same evaporated mass, the last stated parameters of the 1064 nm laser when used for the pre-pulse stage have several disadvantages. First, the laser energy required for the pre-pulse is comparable with the energy of main pulse, and this will significantly decrease the conversion efficiency of the entire system. Second, the maximum temperature of plasma plume developed by the longer wavelength reached 120 eV, while shorter wavelength created plasma with temperature up to 14 eV. Hot plasma with high moving velocities, up to 150 km/s, will have ions with energies up to 12 keV. The ions energy in the plasma created by 266 nm did not exceed 700 eV for this system. Such plasma expanded more uniformly, which created better conditions for EUV emission during the main pulse.

Because the 1064 nm wavelength laser with this intensity created plasmas with high temperatures, the energy redistribution due to radiation fluxes can play significant role in the hydrodynamic evolution of the plasma. We studied the effect of radiation transport on target evolution and modeled self-consistently all phases of laser/droplet interaction, target vaporization, target hydrodynamics, debris ionization, plasma formation and expansion, thermal energy redistribution, and photon generation and transport. Figure 3 shows

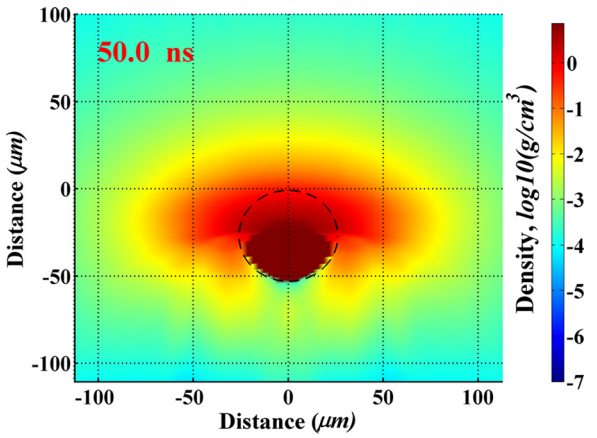

FIG. 1. Mist density from 50-μm droplet created by pre-pulse laser with 266 nm wavelength, ~10 mJ, 50 μm spot. Dotted line shows initial shape of droplet.

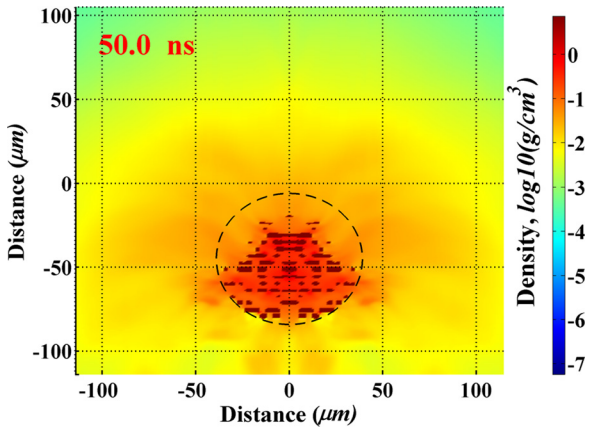

FIG. 2. Mist density from 50-μm droplet created by pre-pulse laser with 1064 nm wavelength, 400 mJ, 100 μm spot. Dotted line shows initial configuration of fragmented droplet.

vaporization dynamics and the contribution due to direct laser photons and to plasma, i.e., with and without the effects of RT. After the initial evaporation of sufficient mass layer needed for efficient laser absorption and the initiation of ionization processes, all laser photons are absorbed within this initially developed plasma/vapor plume. Photons generation in evolving plasma and their transport to the condensed target during and after the laser pulse caused most target vaporization. The influence of plasma radiation on vaporization rate is more pronounced for CO_2 laser even at low intensity, around 10^{10} W/cm^2, where more than 90% of evaporated mass was due to plasma radiation interaction with target (Fig. 4). The last example demonstrates the important effects of incorporating detailed RT on mist plume evolution from the distributed fragments, and as a result on EUV photons source dynamics during the main laser pulse.

Intensive evaporation of small fragments heated by radiation fluxes from the surrounding plasma leads to the formation of relatively cold dense plasma in the volume occupied by the fragments. Such plasma cannot be an efficient source for the 13.5 nm EUV radiation. The EUV photons emission is possible only from plasma above the target surface with appropriate conditions, which are determined mostly by

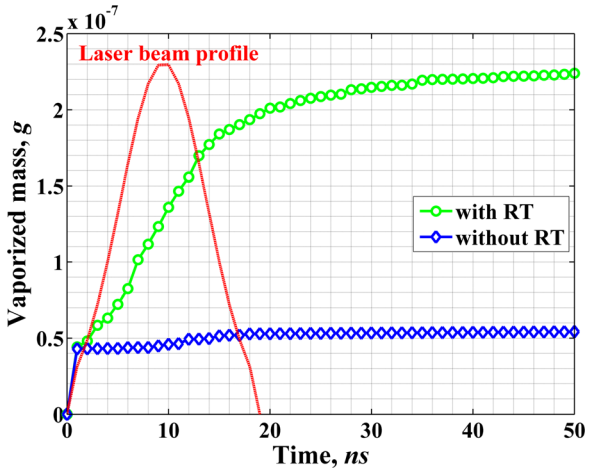

FIG. 3. Vaporization of 50-μm droplet by laser photons and by LPP with 1064 nm wavelength laser, 10 ns FWHM, 400 mJ, 100 μm spot.

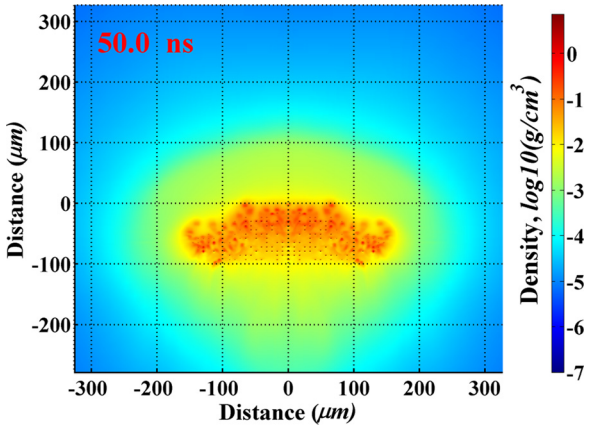

FIG. 4. Mass density evolution of distributed fragments after CO_2 laser pulse heating with total mass equivalent to 50 μm droplet.

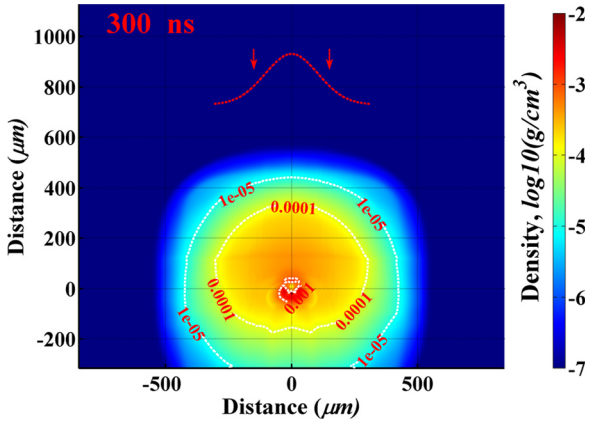

FIG. 6. Mass density distribution developed by 266 nm laser from 20 μm droplet at optimum delay time for efficient coupling with CO_2 laser with 300 μm spot size.

plasma region having temperature around 30–40 eV. Due to plasma plume expansion, the region with optimum conditions for EUV emission also moves away from the surface and this movement is more pronounced in the case of CO_2 laser because of the lower critical density and the usual long pulse duration of this laser. Such dynamics of EUV source produced from the larger area of distributed fragments resemble the high EUV emission and collection from a planar target and, as it will be shown later, these targets yield the same CE for the optimized parameters of the laser beam.

IV. SOURCE OF EUV EMISSION AND EUV POWER AT INTERMEDIATE FOCUS

We analyzed the dependence of CE on the delay time between pulses, on main laser energy, and on spot size for dual-pulse systems using 50-μm droplet as the initial target. Laser with 266 nm was used for initial mist creation from the 50-μm droplet. This laser vaporized about half of the droplet with intensity of 2×10^{10} W/cm^2 and 20 ns duration. We can neglect target fragmentation in this case and consider the target as single droplet during the pre-pulse laser and subsequent time of plume expansion since such low pre-pulse laser intensity cannot cause significant droplet fragmentation.[13] Next, exploring various parameters of the main laser, we found that 500 ns delay is an optimum time for mist expansion for efficient coupling with the incoming main CO_2 laser. Comparative analysis of mass density for optimized EUV output obtained from 50 μm, 20 μm, and 10 μm droplets showed that mist plume should have density of the order of or higher than 10^{-4} g/cm^3 to prevent laser energy loss due to laser photons transmission through matter (Figs. 5–7).

We obtained a maximum CE of about 1.3% in the case of 10 μm droplet and Fig. 7 demonstrates that this value cannot be increased for such small target since the entire droplet was vaporized, mist was uniformly distributed, and plume matched the spot size of main laser that created the best possible conditions for EUV output from this droplet.

To further analyze the above requirements for mist density, we simulated the heating of a large 50-μm droplet by CO_2 laser assuming droplet fragmentation during the pre-pulse stage and fragments distribution to a surrounding volume within 300-μm diameter and then studied the effect of the background density on CE. Fragments with size $\sim$1 μm were randomly distributed in an ellipsoidal volume with the assumed surrounding plume of vapor/plasma. The volume of surrounding plume was varied. We simulated, for the first

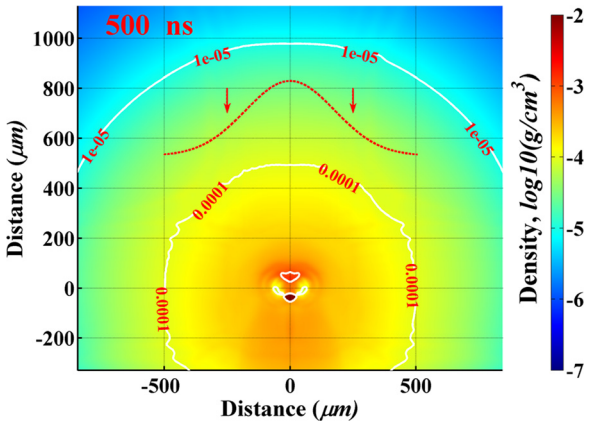

FIG. 5. Mass density distribution developed by 266 nm laser from 50 μm droplet at optimum delay time for efficient coupling with CO_2 laser with 500 μm spot size.

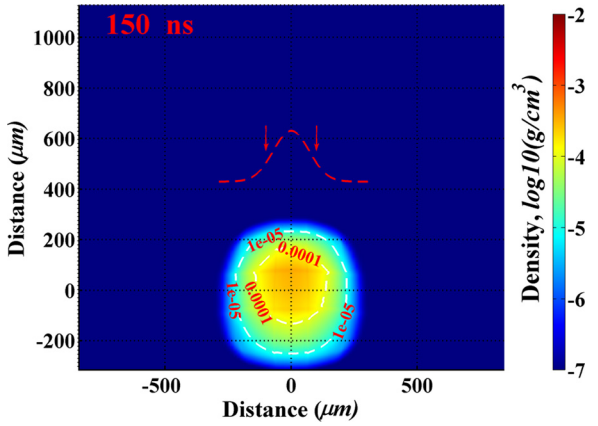

FIG. 7. Mass density distribution developed by 266 nm laser from 10 μm droplet at optimum delay time for efficient coupling with CO_2 laser with 200 μm spot size.

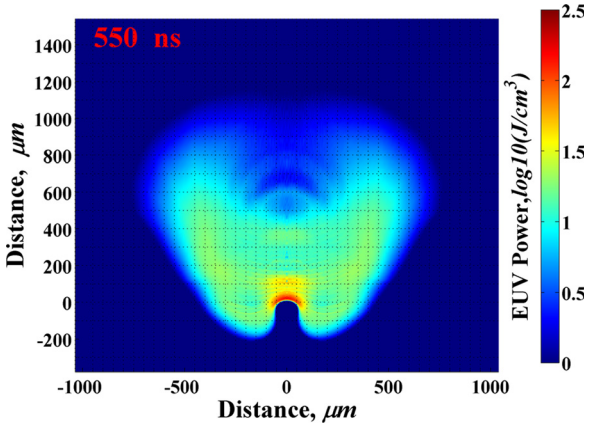

FIG. 8. EUV source from 50-μm droplet preheated by 266 nm laser and distributed during 500 ns. Main laser is CO_2 with 500 μm spot and 350 mJ.

time, the entire processes of laser interaction with the distributed fragments and with vapor/plasma, taking into account laser photons and plasma photons absorption, reflections, and reabsorption after reflection in liquid/vapor/plasma phases. These results showed the same tendency in the requirements for background density, i.e., 10^{-4} g/cm^3 mass density occupying volume of around 10^{-3} cm^3, produced EUV source with 3.3% CE while 10^{-5} g/cm^3 background density produced 2.1% maximum CE, that is the same as from planar target. Matching of laser spot size to the area of fragments distribution in radial direction is very important in the last case.

We also investigated the potential use of the larger droplet size with higher laser power to significantly increase the EUV output at the intermediate focus. We calculated the EUV source size obtained from pre-plasma developed by 266 nm laser and distributed during 300 ns and 500 ns giving the optimum delay time for the considered 20- and 50-μm droplets and pre-pulse parameters. Figures 8 and 9 show EUV source size, location, and intensity (logarithmic values) collected in 5.5 sr during the main laser pulse in plasmas created from 50 μm and 20 μm droplets, respectively. We obtained 11 mJ of EUV energy collected in 5.5 sr in the LPP system using the larger droplet and only 3.5 mJ using the smaller droplet. Taking into account Gigaphoton optical system parameters,[14] EUV power of 600 W and 190 W, respectively, can be generated at the intermediate focus for 100 kHz laser system. This is very encouraging results for potential expansion to higher EUV power from current LPP system design.

Larger droplets do yield higher CE and offer an opportunity for substantial potential increase of source power. However, larger source sizes could have difficulties in efficient EUV photons collection due to current requirements for etendue of the optical system.[15] Also, debris produced from the non-vaporized part of the droplet can significantly decrease chamber components and optical system lifetime. Therefore, more detailed investigation of droplets with sizes starting from 25 μm is needed to get efficient EUV source with minimum contamination and least damage to LPP chamber components.

V. ENERGETIC IONS GENERATION AND MLM SURFACE DAMAGE

To accurately evaluate the potential damage of MLM optical collection system by the energetic tin ions, we calculated the energy spectra of ions produced in both single CO_2 laser and dual-pulse systems and compared our HEIGHTS results with our recent experiments at CMUXE laboratory. We found very good agreement between our modeling and the experimental data[16] as shown in Figs. 10 and 11. These results can be used as additional benchmarking of the HEIGHTS package and predict initial debris parameters for the simulation of Sn ions interaction with mirror surface using our ITMC-DYN code for ions/target interaction.[10]

As it can be seen from Figs. 10 and 11, the single CO_2 laser pulse system produces much more energetic Sn debris than the Nd:YAG due to the nature of energy deposition and the lower critical density for laser absorption. Hot front plasma created by the single CO_2 laser pulse produces ions with energy peaking around 3 keV. In the dual pulse case, the interaction of the CO_2 main laser pulse with the plasma created by the pre-pulse 266 nm laser helped dissipate the CO_2 main energy deeper into the pre-pulse plasma. The produced ions energy in the dual pulse system has a peak only around 30 eV. These unique results demonstrate the

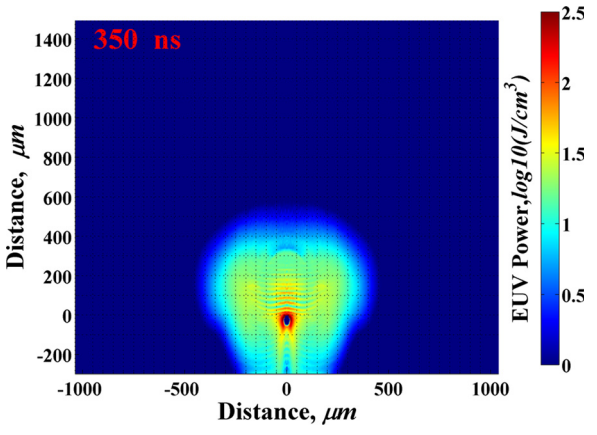

FIG. 9. EUV source from 20-μm droplet preheated by 266 nm laser and distributed during 300 ns. Main laser is CO_2 with 300 μm spot and 140 mJ.

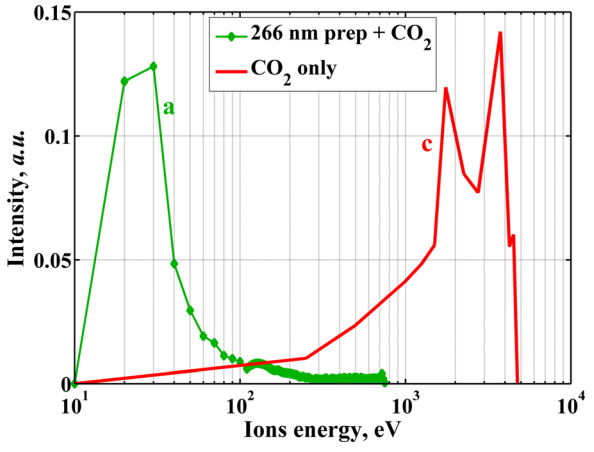

FIG. 10. Ions kinetic energies of HEIGHTS modeling of planar Sn target; 15 mJ for pre-pulse and 90 mJ for CO_2 laser.

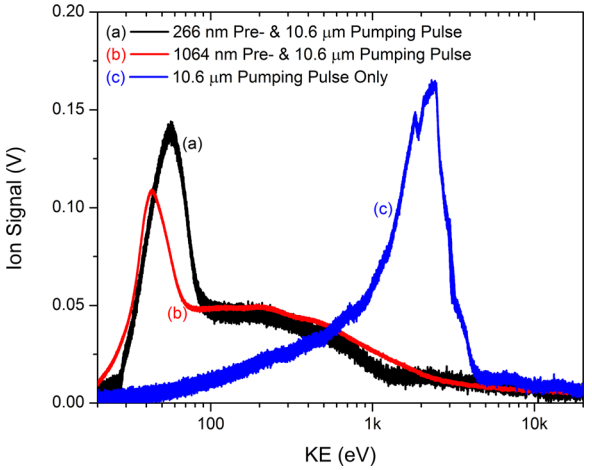

FIG. 11. Ions kinetic energies in CMUXE experiments from planar Sn target; 15 mJ for pre-pulse and 90 mJ for CO_2 laser. Reprinted with permission from Freeman *et al.*, Appl. Phy. A **110**, 853 (2013). Copyright 2012 Springer.

importance of detailed inclusions of various processes in LPP devices during different phases of laser-target interactions.

We then studied using our ITMC-DYN package the interaction of Sn ion fluxes predicted from HEIGHTS simulation and verified by CMUXE experiments with several layers of the MLM surface that consisted of 4.1 Si and 2.8 nm Mo alternating layers[17] with 3 nm Ru coating/capping layer at the surface.[18]

In the case of dual-pulse system, the pre-pulse laser with relatively low intensity did not produce high fluence of energetic ions. In the developed mist plume, the main CO_2 laser photons interacted mainly with plasma surrounded by relatively dense region that prevented producing ions with high kinetic energies. The single pulse device using CO_2 laser in vacuum conditions of the LPP chamber produced plasma with much more energetic ions that can cause serious damage of mirror layers. The damage to MLM surfaces, which reduces mirror reflectivity of EUV photons, can result from either surface deposition or erosion as well as interatomic mixing of the first few layers of MLM system. Ions with low

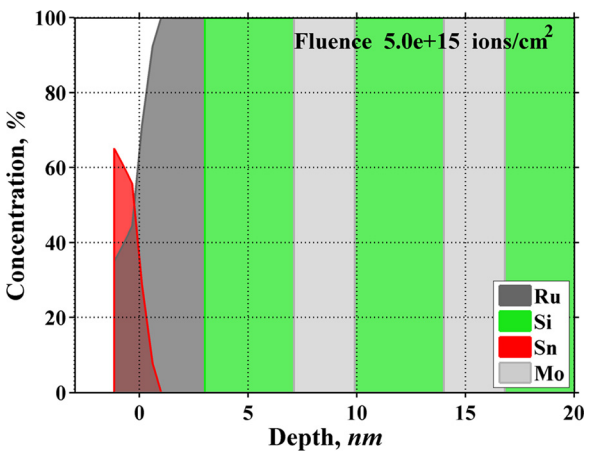

FIG. 12. MLM surface response to Sn ions with Gaussian distribution of energies around 50 eV.

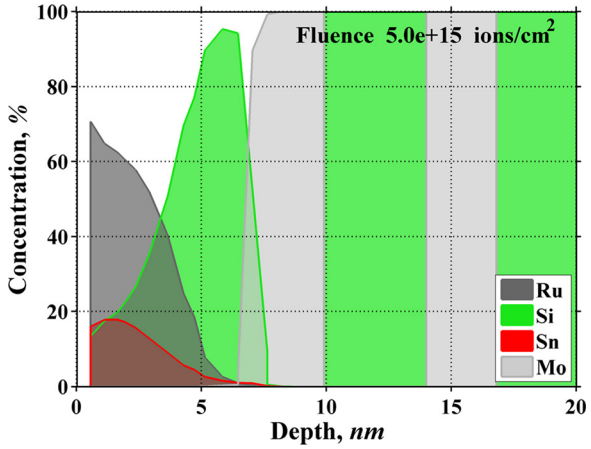

FIG. 13. MLM surface response to Sn ions with Gaussian distribution of energies around 2.5 keV.

energy will interact mainly with the first coating layer, due to Sn deposition on the surface, buildup, and mixing with Ru capping layer as illustrated in Fig. 12. However, ions with 1–3 keV energy can cause substantial erosion of Ru layer, tin implantation to deeper layers, and mirror interlayers mixing that can significantly degrade mirrors reflectivity as shown in Fig. 13.

VI. CONCLUSION

We studied and analyzed LPP sources using different 10–50 μm tin droplet targets, as single droplets as well as distributed microdroplets with equivalent mass, to study mass dependence, laser parameters requirements, atomic and ionic debris generation, and to optimize EUV radiation output. Accurate computer simulation with sufficient details can be used with confidence to understand, design, and optimize LPP plasma devices and save significant time and cost compared to conducting numerous expensive experiments. We extensively benchmarked HEIGHTS package and achieved good agreement with recent experimental results at CMUXE Lab regarding the dependence of ion debris energies on lasers parameters. Laser with shorter 266 nm wavelength for pre-heating Sn droplets results in higher vaporization rate and lower temperatures of plasma plume. The higher vaporization rate allows near complete droplet vaporization and the lower temperatures of plasma plume reduce the fluence and energy of ions debris. The ITMC-DYN simulation showed that ions with low energy, in the order of 30–50 eV, would interact only with first coating layer through Sn deposition on the surface and mixing with Ru capping layer. Energetic ions having 2–3 keV kinetic energy can, however, cause severe erosion of Ru layer, tin implantations to deeper layers, and layers mixing at interface of the MLM system. This can cause significant degradation and loss of mirrors reflectivity. Larger droplet, 50 μm for example, can result in higher CE and offer reasonable pathway for potential increase in source power. However, larger source sizes may have difficulties in efficient EUV photons collection within the given etendue limits. Therefore, more detailed investigation of droplets with sizes starting from 25 μm is needed for designing

efficient EUV sources with minimum debris contamination and least damage to LPP chamber components.

ACKNOWLEDGMENTS

This work was partially supported by the College of Engineering, Purdue University. We gratefully acknowledge the computing resources provided by the Fusion cluster operated by the Laboratory Computing Resource Center at Argonne National Laboratory.

[1]T. Tomie, J. Micro/Nanolith. MEMS MOEMS **11**(2), 021109 (2012).
[2]T. Sizyuk and A. Hassanein, J. Appl. Phys. **112**, 033102 (2012).
[3]T. Sizyuk and A. Hassanein, Phys. Plasmas **19**, 083102 (2012).
[4]V. Sizyuk, A. Hassanein, and T. Sizyuk, J. Appl. Phys. **100**, 103106 (2006).
[5]G. Miloshevsky, V. Sizyuk, M. Partenskii, A. Hassanein, and P. Jordan, J. Comput. Phys. **212**, 25–51 (2006).
[6]V. Sizyuk, A. Hassanein, V. Morozov, and T. Sizyuk, Report No. ANL-MCS-CPH-06/56 (Argonne National Laboratory, 2006).
[7]V. Tolkach, V. Morozov, and A. Hassanein, Report No. ANL-ET/02-23 (Argonne National Laboratory, 2002).
[8]A. Hassanein, G. L. Kulcinski, and W. G. Wolfer, Nucl. Eng. Des. Fusion **1**, 307–324 (1984).
[9]A. Hassanein and D. L. Smith, Nucl. Instrum. Method Phys. Res. B **13**, 225 (1986).
[10]T. Sizyuk and A. Hassanein, J. Nucl. Mater. **404**, 60–67 (2010).
[11]J. Fujimoto, T. Hori, T. Yanagida, T. Ohta, Y. Kawasuji, Y. Shiraishi, T. Abe, T. Kodama, H. Nakarai, T. Yamazaki, and H. Mizoguchi, Proc. SPIE **8322**, 83220F (2012).
[12]A. Hassanein, V. Sizyuk, T. Sizyuk, and S. Harilal, J. Micro/Nanolith. MEMS MOEMS **8**(4), 041503 (2009).
[13]S. Fujioka, M. Shimomura, Y. Shimada, S. Maeda, H. Sakaguchi, Y. Nakai, T. Aota, H. Nishimura, N. Ozaki, A. Sunahara, K. Nishihara, N. Miyanaga, Y. Izawa, and K. Mima, Appl. Phys. Lett. **92**, 241502 (2008).
[14]H. Mizoguchi, T. Abe, Y. Watanabe, T. Ishihara, T. Ohta, T. Hori, T. Yanagida, H. Nagano, T. Yabu, S. Nagai, G. Soumagne, A. Kurosu, K. M. Nowak, T. Suganuma, M. Moriya, K. Kakizaki, A. Sumitani, H. Kameda, H. Nakarai, J. Fujimoto, Proc. SPIE **7969**, 796908 (2011).
[15]V. Bakshi, *EUV Sources for Lithography*, edited by V. Bakshi (SPIE Press, 2005), p. 13.
[16]J. R. Freeman, S. S. Harilal, A. Hassanein, and B. Rice, Appl. Phys. A **110**, 853 (2013).
[17]V. Bakshi, *EUV Lithography*, edited by V. Bakshi (SPIE Press, Bellingham, Washington, USA, 2009), Chap. 7, p. 333.
[18]S. Bajt *et al.*, J. Microlithogr., Microfabr., Microsyst. **5**(2), 023004 (2006).